ALTISSIMO CONSULTING

Road Surface Noise

Influence of Void Fraction on Tyre/Road Noise

Client: NZ Transport Agency - Waka Kotahi
Date: 29th April 2024
Ref: 23-117-R02-C

Prepared for (the Client)
NZ Transport Agency – Waka Kotahi

Prepared by the Consultant)
Altissimo Consulting Ltd

Project	Road Surface Noise
Report	Influence of Void Fraction on Tyre/Road Noise
Reference	23-117-R02-C

Prepared by

George Bell
Consultant

Reviewed by

Robin Wareing
Principal Acoustic Engineer

Version history:

Version	Date	Comment
A	18-03-2024	Release for client review.
B	08/04/2024	Updated following client feedback.
C	29/04/2024	Updated following client feedback.

Report disclaimer and limitations:

This report has been prepared in accordance with the usual care and thoroughness of the consulting profession for the use of the Client. It is based on generally accepted practices and standards at the time it was prepared. No other warranty, expressed or implied, is made as to the professional advice included in this report.

This report should be read in full. No responsibility is accepted for use of any part of this report in any other context or for any other purpose or by third parties. This report does not purport to give legal advice. Legal advice can only be given by qualified legal practitioners.

Abstract

This analysis investigated the influence of porosity, specifically void fraction, on tyre/road noise as a continuation of research efforts by Waka Kotahi. The study explored the hypothesis that the porosity of porous asphaltic mix surfaces plays a significant role in noise generation and attenuation mechanisms. Utilising a nuclear densometer (NDM), the relative void fractions across various asphaltic mix surface types were quantified and the impact on tyre/road noise was explored.

The trial mixes on CNC (SMA, low voids, high strength, and standard porous asphalt) had the expected mean void fraction rankings, except for the SMA, which had a similar mean void fraction to the low voids mix. The trial sections on S2G (standard porous asphalt and high voids) had the expected rankings with the high voids section exhibiting a relatively greater mean void fraction. The thickness trial sites on WBB (EPA7 30, 40 and 50 mm) had similar mean void fractions, with the 30 mm section having a slightly lower mean void fraction than the adjacent 40 and 50 mm sections.

It was observed within the EPA7 (30 mm) and PA7 (30 mm) sections on CNC that the void fractions within the shoulder were consistently greater than the immediately adjacent left wheel path. The mean delta was greater for the conventional compared to the epoxy modified porous asphalt.

The presence of porosity in the asphalt layer is a significant contributor to low-noise performance. The mechanisms by which porosity reduces noise are by increasing the acoustic absorption of the surface and allowing air to be dispersed into the top layer.

While no direct relationship between overall tyre/road noise and void fraction was present in the collected data, there is evidence of negative correlations in the 1,250 to 5,000 Hz bands, which could possibly be attributable to increasing air flow permeability and/or acoustic absorption.

Contents

Abstract ii
Glossary iv
1 Introduction 1
2 Data and Measurements 2
2.1 Void Fraction 2
2.2 Other Data 7
3 Results and Discussion 8
3.1 Void Fraction by Surface Types and Projects 9
3.2 Wheel Path versus Shoulder 11
3.3 Lanes 11
3.4 Thickness 12
3.5 Site-to-Site 13
3.6 Texture 14
3.7 Tyre/Road Noise 15
4 Future Research 18
5 Conclusions 19
6 Preliminary Discussion of Mechanisms 20
References 22
Appendix A – Additional Data 23
Appendix B – Road IDs and Reference Stations 25
Appendix C – Lane Labelling 26

Glossary

CNC	Christchurch Northern Corridor
CPX	Close proximity
CSM2	Christchurch Southern Motorway – Stage 2
EPA	Epoxy-modified porous asphalt
HSD	High speed data
Lane 1	Closest lane to the centre of the road (see Figure 11).
Lane 2	Second-closest lane to the centre of the road (see Figure 11).
L_{CPX}	Close proximity sound pressure level
LWP	Left wheel path
ML	Machine learning
MPD	Mean profile depth
NB	Northbound
NDM	Nuclear densometer
NMAS	Nominal maximum aggregate size
PA	Porous asphalt
PA7 HS	Porous asphalt high strength
RS	Reference station
RWP	Right wheel path
S2G	SH1 Johns Road from The Groynes to Sawyers Arms Road
SB	Southbound
SEM	Standard error of the mean
SMA	Stone mastic asphalt
P1	Standard reference test tyre (passenger tyre)
WBB	Western Belfast Bypass

1 Introduction

This study is a continuation of research into tyre/road noise led by Waka Kotahi (Noise and Vibration Research | Waka Kotahi NZ Transport Agency). The aim of this work was to extend the current understanding of tyre/road noise by examining the variation and influence of porosity of porous asphaltic mix surfaces.

The porosity of a surface influences several of the dominant noise generation and attenuation mechanisms. Surface voids make up a component of the texture, which excites the tyre (Fong, 1998). The ability to disperse air through the surface acts to reduce air pumping noise (Sandberg & Ejsmont, 2002). The porosity is integral in the acoustic absorption of the surface (Berengier et al., 1990).

The porosity of a surface can be simplified into two parameters, (1) void shape, and (2) void fraction. Both parameters influence the aforementioned mechanisms. It is not practical to observe the void shape in situ, however the void fraction can be readily obtained by measuring the density of the asphalt layer using a device such as a nuclear densometer (NDM).

The NDM is a tool for measuring the density of asphalt surfaces. The methodology is prescribed in AS/NZS 2891. 14.2:2013. The basic principle of the NDM is to emit radiation and measure the reflections. The amount of radiation that is absorbed or scattered by the asphalt surface is directly proportional to the density. The total void fraction is calculated by dividing the measured density by the theoretical maximum density. The interconnected void content may potentially be more pertinent to tyre/road noise; however, there are no non-destructive methods known to the author that can rapidly and economically quantify the inter-connected void fraction.

The objectives of this investigation were to:

- Quantify the relative void fractions for a range of asphaltic mix surface types.
- Explore the variation of void fraction for different positions on the road.
- Explore how tyre/road noise is influenced by void fraction.

This report includes a description of the density measurements and other data sources, followed by concurrent presentation and discussion of the results. A preliminary discussion of how noise generation and attenuation mechanisms may be affected by void fraction is included at the end of this report.

2 Data and Measurements

2.1 Void Fraction

2.1.1 Instrument

The Road Science NDM was used for all measurements. The NDM details are given in Table 1. A photo of the NDM on the road during testing is shown in Figure 1.

Table 1: Road Science NDM details.

Model	Serial No.	Last Calibration Date	Next Calibration Date
Troxler 46440B	2696	10-10-2022	10-10-2024

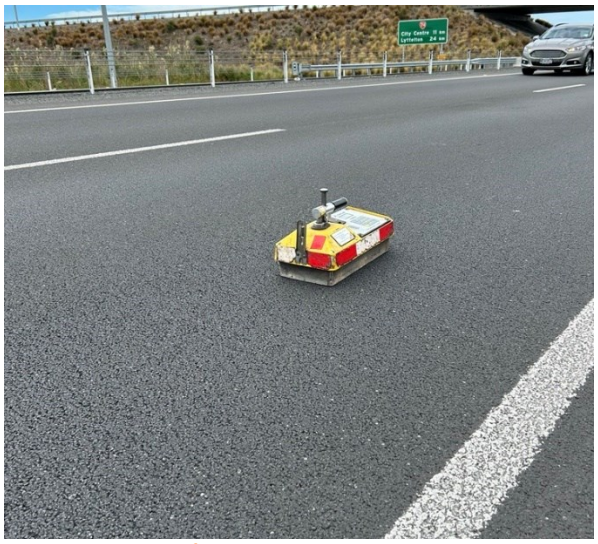

Figure 1: Photo of the NDM on the road during measurements.

2.1.2 Measurement Method

For each measurement, the following steps were taken:

1. The measurement location was visually inspected for irregular surface deformation (e.g., scrapes, holes, cracks, etc.) and loose debris (e.g., free stones). Locations where the surface was deformed were not measured. Loose debris was removed.
2. The NDM measurement was commenced with the following parameters:
    a. Measurement duration: 60 seconds
    b. Measurement depth: The greater of either 25.4 mm, or 5 mm less than the specified thickness (e.g., for a specified thickness of 50 mm, a depth of 45 mm was used). For CNC measurements only, the actual minimum thickness (measured using a laser survey) for a given section was used. Where the actual thickness was less than 25.4 mm, the measurement was omitted from the results.

2.1.3 Samples

Measurements were taken across several projects and surface mixes. The projects and their respective surfacing and measurement dates, and age are given in Table 2. Measurements were undertaken in dry conditions during the daytime. Four days of measurements were undertaken over a five-month period. The measurements for CNC spanned a three-month period, it was assumed that no significant changes in the void fraction occurred during this time.

Table 2: Projects, measurement and surfacing dates, and age at the time of measurement.

Project	Measurement Date	Surfacing Month(s)	Age - Years
CNC	28-11-2023	Feb-Mar 2022	1.8
	20-02-2024		2.0
	21-02-2024		2.0
S2G	03-10-2023	Mar 2017	6.5
WBB	03-10-2023	Nov 2018	4.8

A total of 576 measurements were performed and consisted of points in the shoulder, and the left wheel path within the left and right lanes. The number of samples for each project, surface type, and position are given in Table 3. Within the wheel path, longitudinal spacings of 1, 10, and 20 m were used; the spacings by surface type and location are given in Table 9 in Appendix A. Shoulder measurements were conducted approximately 0.3 m from the edge line next to the location where wheel path measurements were made. These measurements across the shoulder area were evenly distributed along the measurement sections (e.g., a 300 m section with three shoulder measurements would have samples at 0, 150, and 300 m). High spatial resolution shoulder measurements, specifically at 10 m and 20 m, were performed on the PA7 (30 mm) and EPA7 (30 mm) surfaces on CNC.

Table 3: NDM measurements by project, surface type, and position.

Project	Surface Type	Position	Samples
CNC	EPA7 (30 mm)	Lane 2	63
		Shoulder	23
	EPA7 (50 mm)	Lane 1	38
		Lane 2	92
		Shoulder	3
	PA7 (30 mm)	Lane 2	70
		Shoulder	23
	PA7 HS (30 mm)	Lane 2	17
		Shoulder	2
	PA7 LV (30 mm)	Lane 2	19
		Shoulder	2
	SMA7 (30 mm)	Lane 2	6
S2G	EPA10 (30 mm)	Lane 2	49
		Shoulder	9
	EPA10 HV (30 mm)	Lane 2	30
		Shoulder	5
	EPA14 (30 mm)	Lane 2	14
		Shoulder	6
WBB	EPA7 (30 mm)	Lane 2	26
		Shoulder	4
	EPA7 (40 mm)	Lane 2	26
		Shoulder	6
	EPA7 (50 mm)	Lane 2	39
		Shoulder	4
		Total	**576**

2.1.4 Calculating Void Fraction

The NDM returns the density, which can then be used to estimate the total void fraction. The void fraction (γ) is calculated using Equation 1.

Equation 1

$$\gamma = 1 - \frac{(\rho_M + \rho_S)}{TMD}$$

Where:

ρ_M Measured density – kg/m³

ρ_S Surface void correction – kg/m³

TMD Theoretical maximum density – kg/m³

The TMD for each surface type was taken from the mix designs. The TMD for each surface type is given in Table 4. Note that the same mix design for EPA7 was used across the CNC and WBB projects.

Table 4: TMD for measured surfaces.

Surface Type	TMD kg/m³
EPA7 (30 mm)	2,447
EPA7 (40 mm)	
EPA7 (50 mm)	
EPA10 (30 mm)	2,454
EPA10 HV (30 mm)	2,474
EPA14 (30 mm)	2,478
PA7 (30 mm)	2,432
PA7 HS (30 mm)	2,431
PA7 LV (30 mm)	2,401
SMA7 (30 mm)	2,384

The surface void correction (ρ_S) is used to account for the free air between the bottom face of the NDM and the top surface of the asphalt. A highly simplified diagram of a cross-section of a porous layer is shown in Figure 2. The bottom face of the NDM creates the "Top Plane" formed by the protruding asphalt (i.e., the aggregate). The threshold between surface and sub-surface voids is defined as the depth where the void fraction is not influenced by free air. As the NDM returns the underlying density, which includes all material within the observed penetration depth, a correction must be applied to account for the air in the surface voids. Based on discussions with the NDM operators, a surface void correction of 150 kg/m³ was used for all surface types. It is expected that use of a single value for this correction is an over-simplification as surface voids are likely to vary . A more robust approach would be to derive this correction from volumetric testing of multiple core samples. As this was not undertaken for this study, absolute void fractions must be considered as indicative and not used outside of the analysis described in this report. It is recommended that a future investigation explores the surface void correction possibly through the use of core sampling.

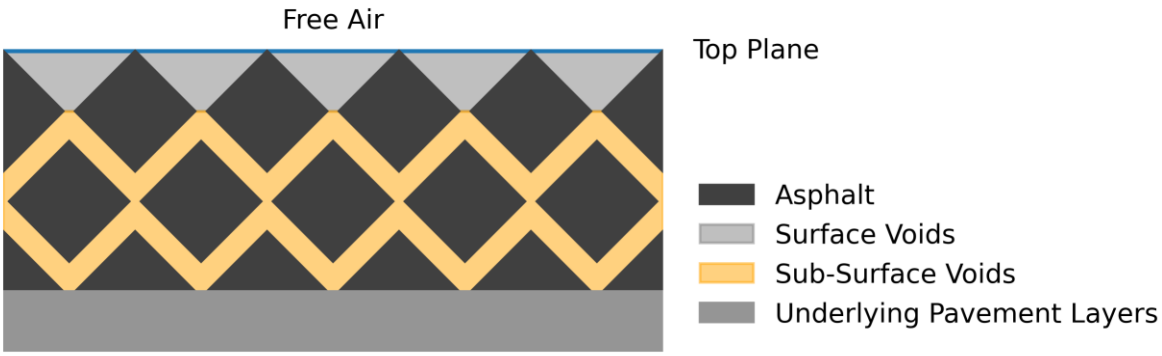

Figure 2: Diagram of a cross-section of a porous asphalt layer.

The void fractions returned by the NDM represent only the sub-surface voids. Unless otherwise stated, when "voids" is used within the remainder of this report it is referring to the total estimated sub-surface void fraction returned by the NDM.

The sensitivity of the void fraction to each input was explored using the one-variable-at-a-time method. A range of ±50 kg/m³ about a baseline value of each input variable was calculated. Nominal values of 1950, 2450, and 150 kg/m3 were used for the measured density, TMD, and surface void correction, respectively. The resulting void fractions as a function of each input variable are given in Figure 3. Perturbations of ±50 kg/m³ of each input variable resulted in a change of up to ±2% of the baseline void fraction (14.3%).

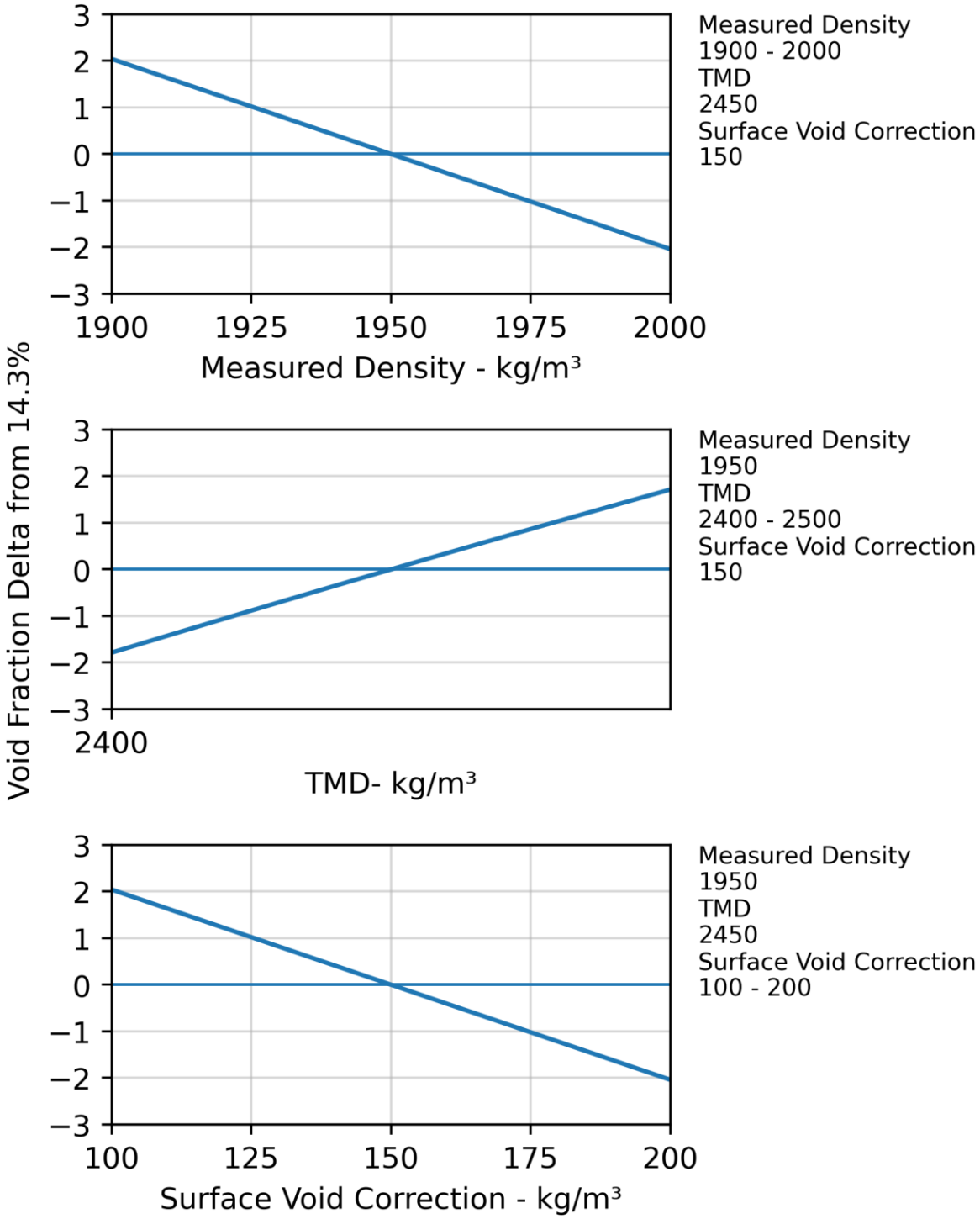

Figure 3: Void fraction sensitivity analysis results.

2.2 Other Data

The details of other data sets used in the analysis are given in Table 5. Note that all CPX data used in this analysis are with the P1 tyre and a speed of 80 km/h ($L_{CPX} = L_{CPX:\,P1,80}$). The texture data was from the annual high-speed data (HSD) survey as this was the only source at the time of analysis; texture data from the laser on the CPX trailer will be available for future studies.

Table 5: Tyre/road noise and texture measurement information.

Data	Source	Longitudinal Resolution	Project	Measurement Date
Tyre/road noise	Waka Kotahi CPX Trailer	4 m	CNC	22-11-2023 (left)
				06-12-2023 (right)
			S2G	22-11-2023
			WBB	22-11-2023
Texture (MPD)	HSD Survey	10 m	CNC	21-01-2023
			S2G	21-01-2023
			WBB	21-01-2023
Thickness	Woods Mobile Survey	0.1 m	CNC	07-2022

3 Results and Discussion

The following analyses were conducted and are presented in this section.

- Void fraction by project and surface type.
- Void fraction delta between the wheel path and shoulder.
- Void fraction differences between lanes 1 and 2.
- Relationship between thickness and void fraction.
- Comparison of the void fraction for surfaces of the same specification at different locations.
- Relationship between void fraction and texture.
- Influence of the void fraction on the overall and one-third octave band L_{CPX}.

The relative values of the void fraction are assumed to be robust for the purpose of this analysis, however, without secondary validation and correction through another method (e.g., core sampling), the absolute levels must be regarded as indicative. Limited reference to the specified void fractions for surfaces are made below; these are only included for context and are not intended to be used to determine if the surfaces met the specified values.

The mean and standard deviation of the void fraction for each project, surface type, and position can be found in Table 10 in Appendix A.

3.1 Void Fraction by Surface Types and Projects

The void fraction for the left wheel path in lane 2 (left lane) of each surface type and project are shown in Figure 4. For context only, the specified void fraction ranges by surface type at the time of construction are given in Table 6. in the open-graded porous asphalt mix design process, both sub-surface and surface voids are included in the specified void fraction. Therefore, the sub-surface void fractions in this report are not directly comparable to the specified void fraction and are expected to be lower.

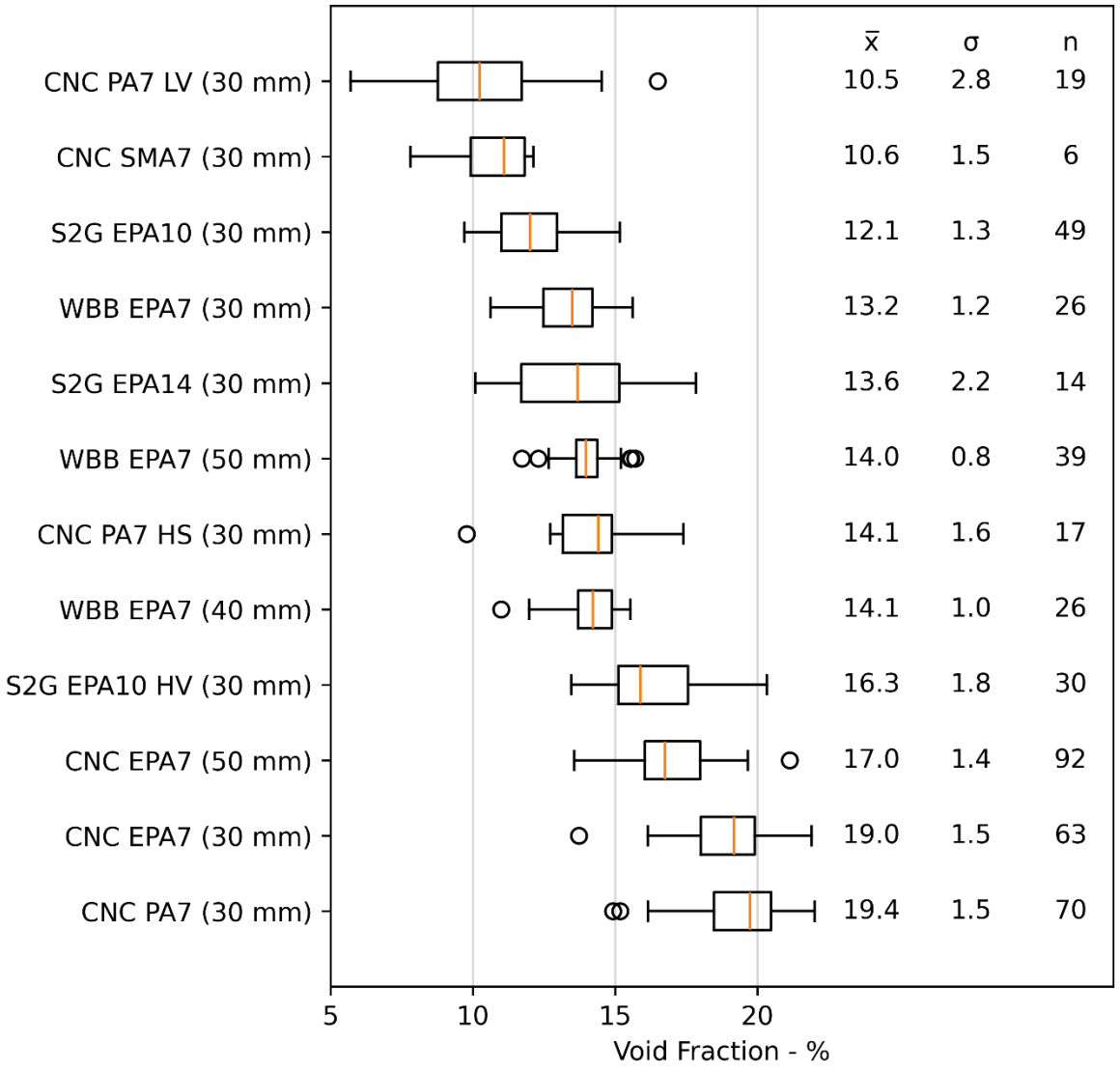

Figure 4: Boxplots of void fraction in the left wheel path of lane 2 by location and surface type.

Table 6: Surface type and specified void fraction.

Surface Type	Specified Void Fraction
SMA	2-6%
PA LV	8-10%
PA HS	12-16%
PA/EPA	20-25%
EPA HV	25-30%

Within the CNC project, the PA7 LV (30 mm) and SMA7 (30 mm) surfaces had the lowest observed mean void fractions of 10.5% and 10.6%, respectively. These were followed by the PA7 HS (30 mm) with a mean void

fraction of 14.1%. The remaining surfaces of EPA7 (50 mm), EPA7 (30 mm), and PA7 (30 mm), had mean void fractions of 17.0, 19.0, and 19.4%, respectively. Excluding the SMA7 (30 mm), the mean void fractions were in the same order as the void fraction specifications. It is understood an issue occurred during the construction of the SMA7 (30mm) that is likely to be the cause of the relatively high void fraction. The SMA7 (30 mm) was a trial section and is not considered to be representative of typical SMA surfaces.

Within S2G, the mean void fractions for the EPA10 (30 mm), EPA14 (30 mm), and EPA10 HV (30 mm) were 12.1, 13.6, and 16.3%, respectively. The mean void fraction of the six-year-old EPA10 HV (30 mm) on S2G was 2.6% lower than that of the two-year-old EPA7 (30 mm) sections on CNC, with a 95% confidence interval of 1.9-3.4%, and the difference was statistically significant (T-Test $p \leq 0.05$). It is recommended that a future investigation explores the cause of the apparent reduced void fraction for the older surface.

Within WBB, the EPA7 (40 mm) and EPA7 (50 mm) surfaces had no significant difference between the mean void fractions (T-Test $p = 0.48$). The mean void fraction of the EPA7 (30 mm) was 0.9% lower than that of the EPA7 (40 mm) and 0.8% lower than that of the EPA7 (50 mm), with corresponding 95% confidence intervals of 0.3-1.6% and 0.2-1.4% - both differences were statistically significant (T-Test $p \leq 0.05$). The observed differences of 0.8 and 0.9% are relatively minor when compared to the specified void fraction range of 5% for porous asphalt (20-25%), suggesting the practical significance may be minimal.

Although the absolute values of the measured void fractions have not undergone validation by a second method, it is assumed that they reflect the relative rankings.

3.2 Wheel Path versus Shoulder

The PA7 and EPA7 (30 mm) measurements from CNC were explored to determine if there was a difference between the void fraction in the shoulder and the adjacent left wheel path in lane 2. Any difference may possibly be attributable to trafficking effects. The distributions of deltas (shoulder minus left wheel path) are shown in Figure 5. For both EPA7 and PA7 (30 mm), the mean void fraction in the shoulder was 2.3% ±0.8% and 3.9% ±0.8% greater than in the wheel path, respectively.

The reason for the reduced void fraction in the wheel path could not be deduced from the available data. It might be due to compaction from trafficking (initially and/or over time), collection of debris in the voids, an artefact of construction (e.g., less compaction in the shoulder), or another factor.

The mean delta for the PA7 (30 mm) was 1.6% greater than that of the EPA7 (30 mm) with a 95% confidence interval of 0.3-2.8%, with a statistically significant difference (T-Test $p \leq 0.05$). Given the indication of a difference it is recommended that the trend is explored further in a future study. An analysis of the tyre/road noise for this location indicated that the L_{CPX} for the EPA7 (30 mm) was 1.0 dB less than the PA7 (30 mm), which was driven by reductiDdons in the mid (1,000-1,600 Hz) and high (3,150-5,000 Hz) frequency bands (Bell, 2024).

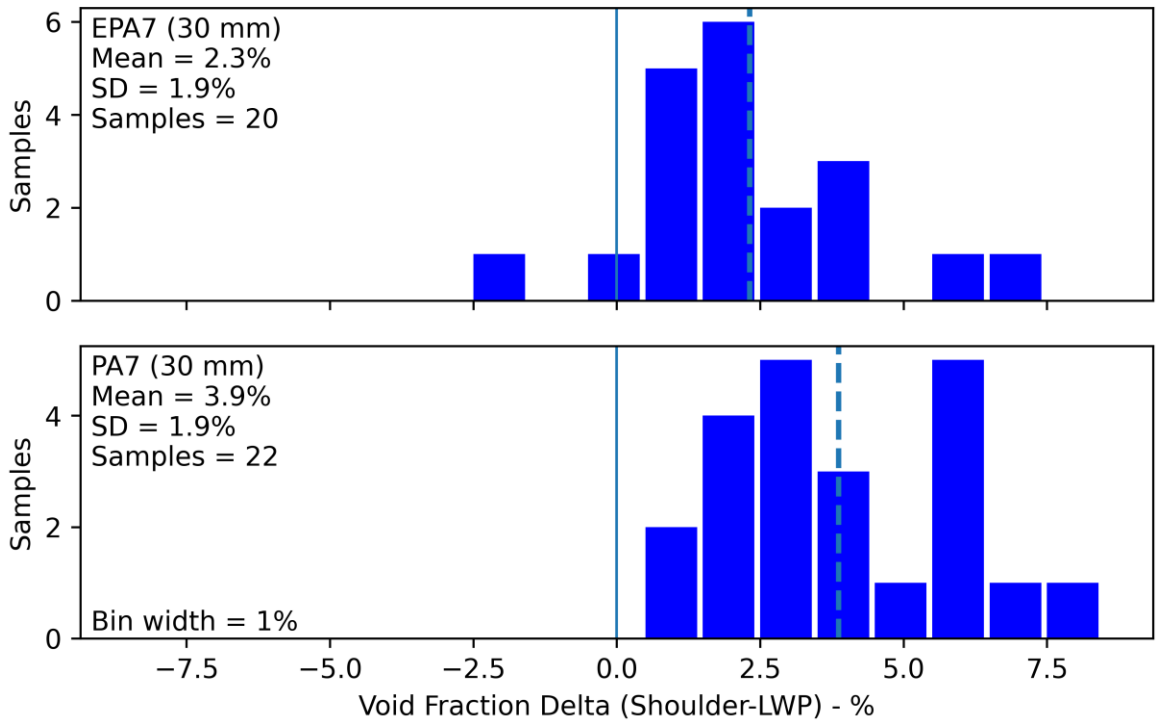

Figure 5: Distributions of shoulder to lane void fraction deltas for EPA7 and PA7 (30 mm) surfaces on CNC.

3.3 Lanes

The void fraction of a 370 m section of EPA7 (50 mm) on CNC was explored to determine if there was a significant difference between lane 1 (right lane) and 2 (left lane). For this single section, the mean void fraction in lane 1 was 2.7% lower than lane 2 with a 95% confidence interval of 2.2-3.3%, the difference was statistically significant ($p \leq 0.05$). The reason for the lower void fraction in lane 1 is unknown. It is recommended that a future investigation expands the investigation of the disparities of lane 1 and 2 as differences in L_{CPX} are not attributable to only thickness and MPD.

3.4 Thickness

The EPA7 surface on CNC was used to explore whether void fraction was correlated with thickness. The local thickness was taken from the high-resolution laser survey. Three thickness bands were used, which included 30, 40, and 50 mm with a tolerance of ± 3 mm. Boxplots of the void fraction for each thickness band are shown in Figure 6. The mean differences, T-Test p-values, and 95% confidence intervals for each pairing of thickness are given in Table 7. The 30 mm band had a greater mean void fraction than the 40 mm and 50 mm bands (2.8 and 2.7%, respectively). There was no significant difference (p = 0.74) between the mean values of the 40 mm and 50 mm bands. The reason for the greater void fraction of the 30 mm band compared to 40 mm and 50 mm on CNC is unknown. Measurement artefacts related to the different depth settings cannot be excluded as a potential cause. The opposite trend was observed on the WBB thickness trial sites (nominally 30, 40, and 50 mm), where the 30 mm surface had a lower (0.9 and 0.8% for the 40 and 50 mm surfaces, respectively) mean void fraction, however no local thickness data was available for WBB so the thickness groups could only be based on the specified values.

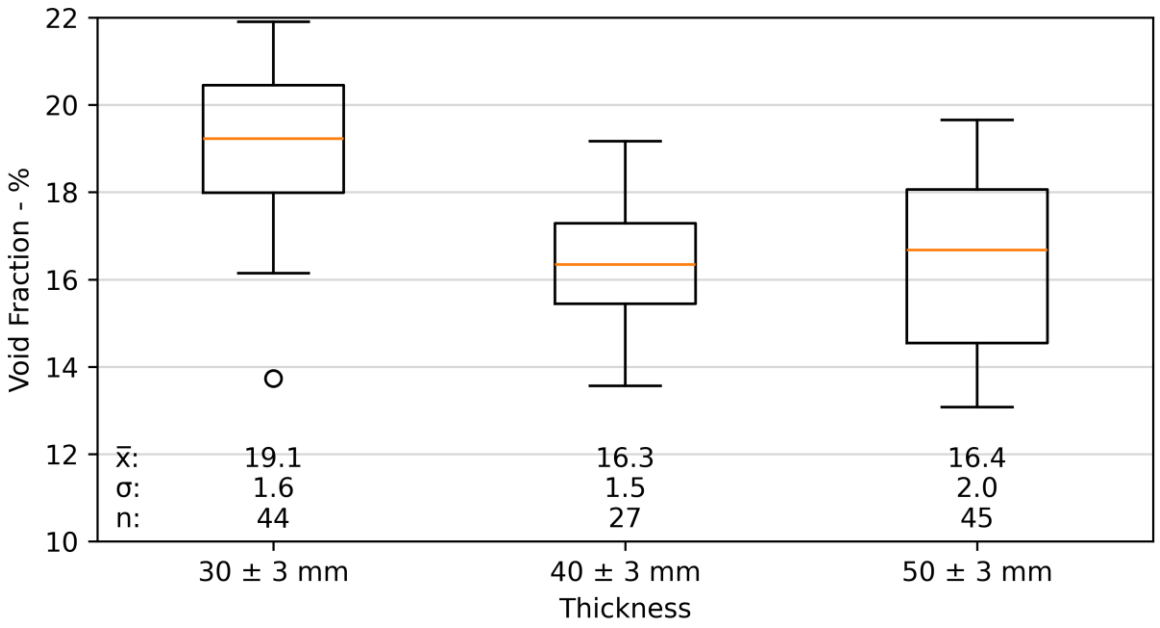

Figure 6: Boxplots of void fraction by thickness for the EPA7 surface on CNC.

Table 7: T-Test p-values, mean differences, and 95% confidence intervals for each pair of thickness bands.

Group 1	Group 2	T-Test P-Value	Mean Difference (Group 1 – Group 2)	Mean Difference 95% CI
EPA7 (30 mm) n = 44	EPA7 (40 mm) n =27	≤ 0.05	2.8	1.9 – 3.4%
EPA7 (30 mm) n =44	EPA7 (50 mm) n =45	≤ 0.05	2.7	2.1 - 3.6%
EPA7 (50 mm) n =45	EPA7 (40 mm) n =27	0.74	-	-

3.5 Site-to-Site

The EPA7 (30 mm) and EPA7 (50 mm) surfaces on CNC and WBB were compared to explore the site-to-site variation of void fraction for the same nominal surface type. The surfaces have different ages of two and five years for CNC and WBB, respectively (where age is the time between surfacing and density measurements). CNC and WBB used the same contractor, aggregate source, and mix design. Note that while the ages of the surfaces at the time of measurement were different, other factors could not be appropriately isolated to consider any resulting differences to be due to age alone.

The mean differences, T-Test p-values, and 95% confidence intervals are given in Table 8. For both the 30 mm and 50 mm samples, the WBB samples had a reduced mean void fraction (5.8% and 3.0% for the 30 mm and 50 mm surfaces, respectively) than the same surface (i.e., as specified) on CNC.

Table 8: T-Test p-values, mean differences, and 95% confidence intervals for each pair of surface types.

Group 1	Group 2	T-Test P-Value	Mean Difference (Group 1 – Group 2)	Mean Difference 95% CI
CNC EPA7 (30 mm) n = 63	WBB EPA7 (30 mm) n = 26	≤ 0.05	5.8%	5.1 – 6.4%
CNC EPA7 (50 mm) n = 92	WBB EPA7 (50 mm) n = 39	≤ 0.05	3.0%	2.6 – 3.4%

There are many factors that could possibly cause the observed differences between these two sites, including age, trafficking, material properties, construction processes, etc. It would be useful to understand how the void fraction changes over time (and the subsequent impact on tyre/road noise, texture, water drainage, etc.); this could be achieved through either a longitudinal or cross-sectional study measuring properties such as density, air flow permeability, and acoustic absorption.

3.6 Texture

The relationship between void fraction and texture was explored. For this analysis, only the texture metric of mean profile depth (MPD) was considered. For porous asphalts, the MPD is influenced by both unevenness arising from the aggregate protruding from the asphalt layer and the voids that are open to free air (see Figure 2 for a simplified diagram of a cross-section of a porous layer).

Figure 7 contains a scatter plot of MPD (from the 2023 HSD survey) as a function of void fraction grouped by the nominal maximum aggregate size (NMAS). A linear regression model was applied between MPD and void fraction for each NMAS. The results from the models indicated a statistically significant ($p \leq 0.05$) positive linear relationship for the 7 mm and 10 mm NMAS groups. The slopes of the linear fits were 0.009 ± 0.001 mm/% and 0.023 ± 0.004 mm/% for the 7 mm and 10 mm NMAS groups, respectively. The coefficients of determination of 0.14 and 0.42 for the 7 mm and 10 mm NMAS groups, respectively, suggest that the variations in the MPD within the NMAS groups can be partially explained by a linear relationship with void fraction. A linear fit was applied to the CNC subset (n = 243) of the 7 mm NMAS group, and a significant relationship was present ($p \leq 0.05$). The slope of the linear fit was 0.018 ± 0.001 mm/%. The coefficient of determination for this subset was 0.43, suggesting that the linear fit was a better predictor for the CNC subset.

It is apparent that the MPD was influenced more by the NMAS than the void fraction for the considered data. For example, a change in void fraction of 10% has a predicted change of 0.09 mm and 0.23 mm in MPD for 7 mm and 10 mm NMAS, respectively, while the predicted increase in MPD between an NMAS of 7 mm to 10 mm at a void fraction of 15% has a predicted increase of 0.38 mm. This example is only intended to illustrate an observation and the values must be considered as indicative. Additional measurements would be required to quantify the relationship between MPD, void fraction, and NMAS.

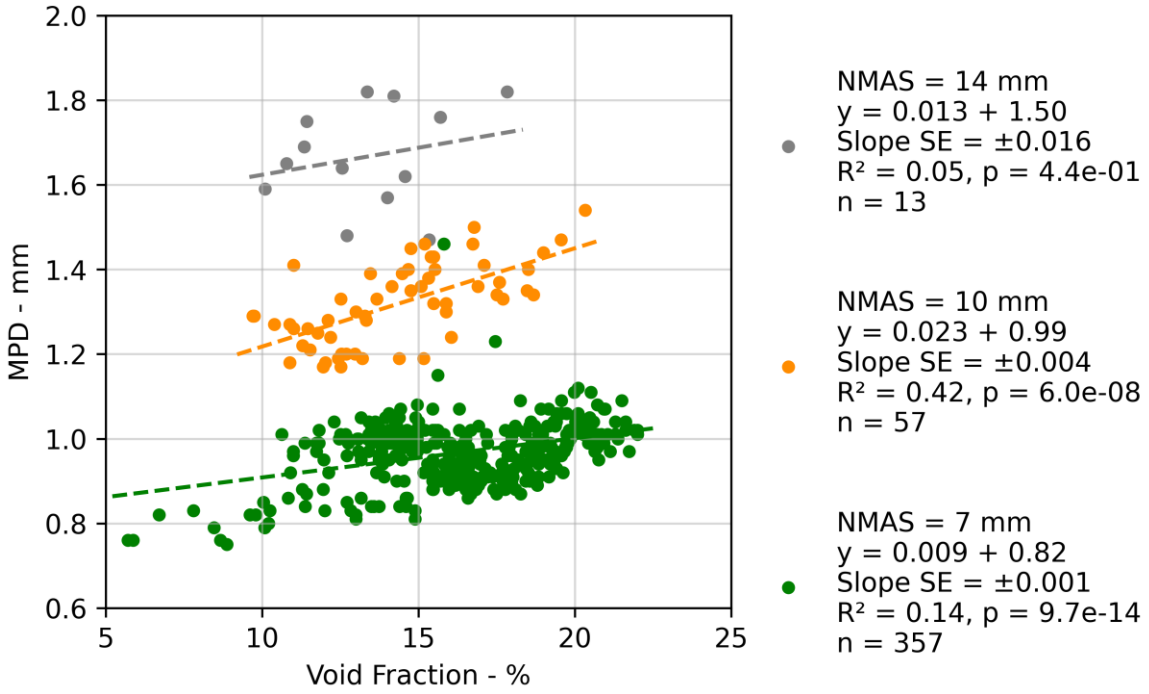

Figure 7: MPD as a function of void fraction for all surfaces.

3.7 Tyre/Road Noise

3.7.1 Overall

The overall L_{CPX} is plotted as a function of void fraction in Figure 8. Linear and polynomial models were applied to determine if a significant relationship existed between the overall L_{CPX} and void fraction for the available data. None of the models exhibited a significant relationship ($p > 0.05$). The lowest LCPX values (89 to 90 dB) in Figure 8 occurred in the left wheel path of lane 1 on the EPA7 (50 mm) on the southbound carriageway of CNC.

A pattern emerged regarding the behaviour of the minimum L_{CPX} values across the measured void fraction range. It was observed that the minimum L_{CPX} presents a trend, characterised by a local minimum at a void fraction between 12.5 and 17.5%. This pattern may indicate the existence of a lower limit to L_{CPX}, which is possibly dependent on the void fraction. This observation is made without asserting the discovery of a definitive relationship. In addition, there may be dependencies between void fraction and other influential parameters (e.g., thickness) that are causing the described trend. It is recommended that a future study explores this phenomenon, potentially employing a multivariate or machine learning (ML) model with void fraction, thickness, and texture.

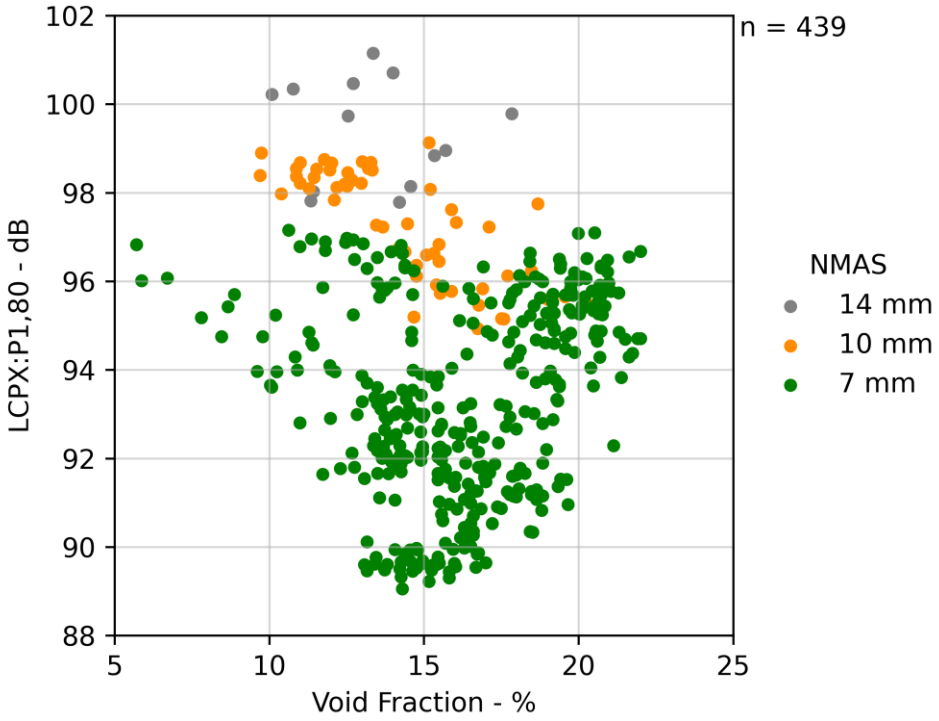

Figure 8: Overall L_{CPX} as a function of void fraction for all measured surfaces.

3.7.2 One-Third Octave Bands

The influence of the void fraction on the one-third octave band L_{CPX} spectra was explored. Linear models were applied between each one-third octave band and void fraction. The resulting slopes of the linear models and R^2 values are shown in Figure 9. Only relationships significant at $p \leq 0.01$ are included. The error bars for the slopes are the standard error for the slope of the linear model. A single example of the 1,600 Hz band as a function of void fraction is given in Figure 10 (this band exhibited the greatest R^2).

The one-third octave bands from 1,250 to 5,000 Hz were negatively correlated with void fraction. Potential mechanisms could include increasing air flow permeability and enhanced acoustic absorption. It is recommended that a multivariate model is used in a future investigation to explore these observations further.

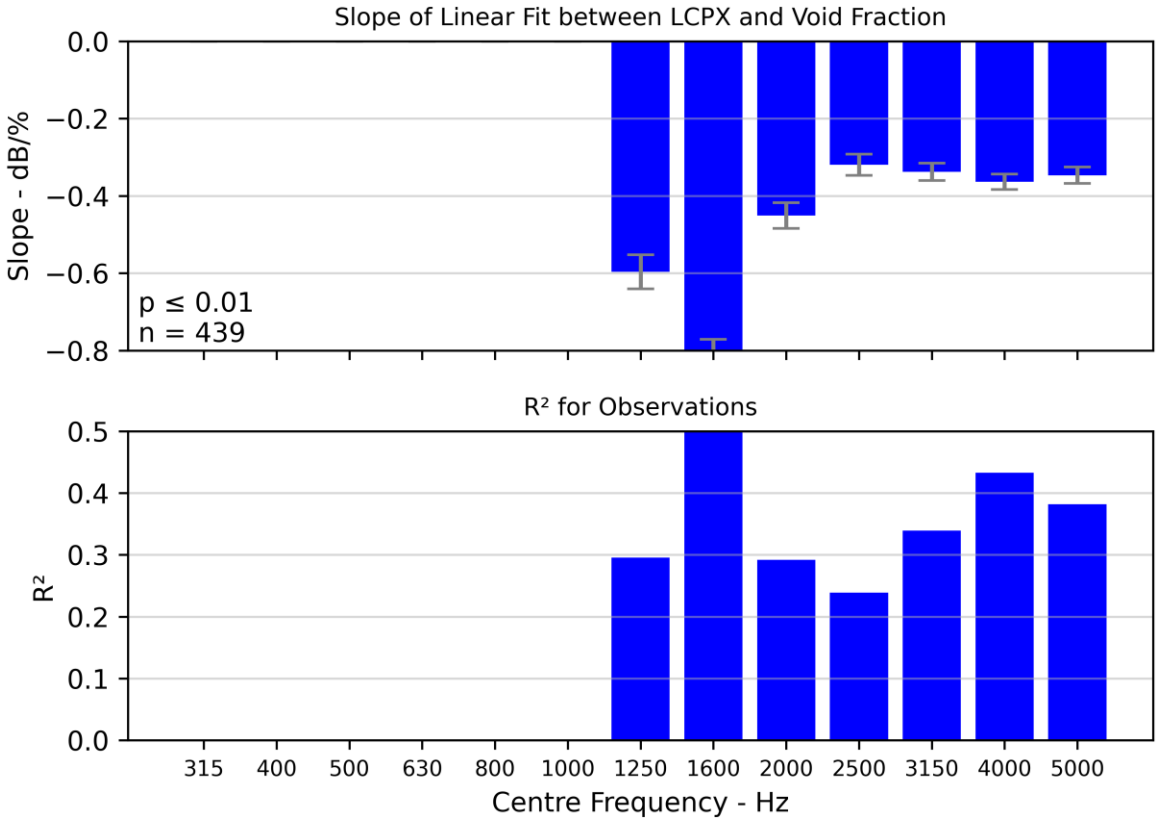

Figure 9: Slopes of linear fits between one-third octave band L_{CPX} and void fraction and the R^2 with the measured data.

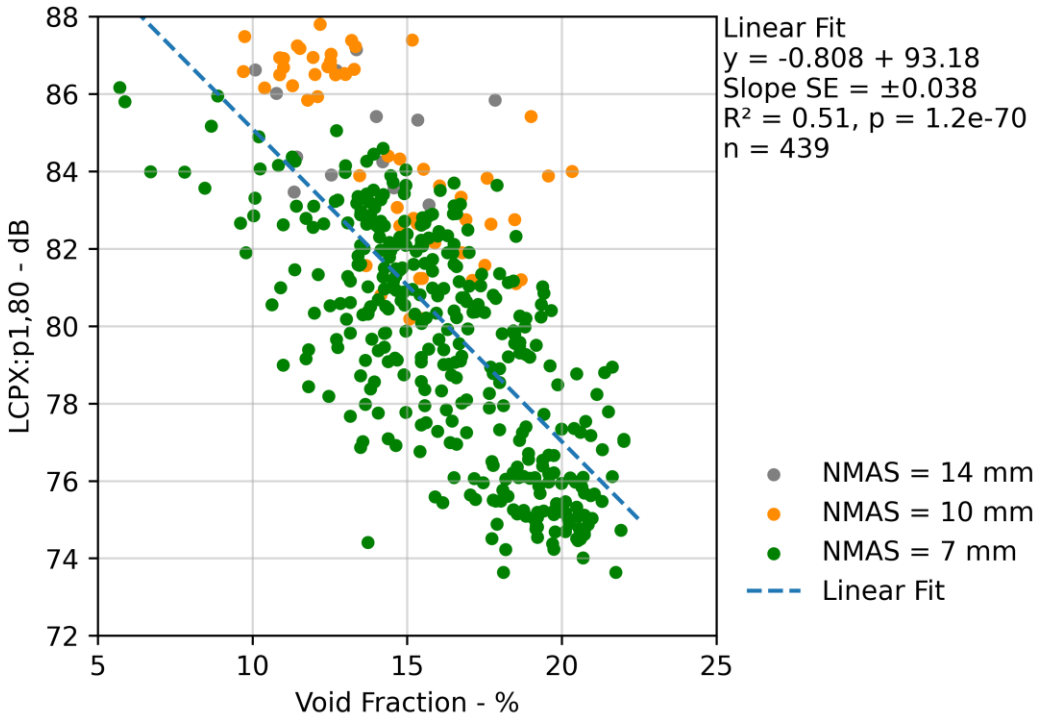

Figure 10: L_{CPX} in the 1,600 Hz one-third octave band as a function of void fraction for all surfaces.

4 Future Research

Based on the findings in this report, the following areas are recommended for further investigation.

- **NDM Validation**

  Compare NDM results to known samples (e.g., lab specimens). Explore the effect of the depth setting.

- **Multivariate Analysis**

  Create a multivariate regression model between L_{CPX}, void fraction, texture, and thickness.

- **Lanes**

  Conduct further density measurements in lane 1 to explore whether there is a significant difference between the void fraction in lane 1 and 2.

- **Thickness**

  Measure the density at another location with local thickness data (e.g., CSM2) to confirm whether the observed trend between thickness and void fraction is not unique to CNC.

- **Short-Term Compaction**

  Measure the density immediately following paving and progressively thereafter to determine when compaction is predominantly occurring.

- **Shoulder and Wheel Path**

  Expand the measurements of adjacent shoulder and wheel path pairs to different surfaces and projects.

- **Change Over Time**

  Measure the density of the same surface specification for a range of ages (i.e., a cross-sectional study). Continue to measure the density of the same surfaces over time (i.e., a longitudinal study)

- **Impervious Surface Proximity**

  Measure the longitudinal density changes immediately following impervious surfaces (e.g., the SMA on CSM2) to determine if debris transfer is accelerating the loss of voids in porous surfaces.

- **Surface Void Correction Prediction from Texture**

  Use validated density results and high-resolution texture measurements to estimate the surface void correction.

5 Conclusions

An NDM was used to measure the density and estimate the void fraction of the surface asphalt layer. A total of 576 measurements were made across three projects and 10 surface types. No other measurement methods were available that could potentially have determined the surface air void correction and validate the absolute NDM density measurements; therefore, the analysis focused on relative changes.

The rankings and relative changes in void fraction were considered for the various surfaces within the CNC, S2G, and WBB projects. The trial mixes on CNC had the expected mean void fraction rankings, except for the SMA7 (30 mm), which had a similar mean void fraction to the PA7 LV (30 mm) section. The trial sections on S2G had the expected rankings with the high voids section exhibiting a relatively greater mean void fraction within that project. The thickness trial sites on WBB had similar mean void fractions, with the EPA7 (30 mm) section having a slightly lower mean void fraction than the adjacent 40 and 50 mm surfaces.

For the EPA7 and PA7 (30 mm) surfaces on CNC, it was observed that the void fraction in the shoulder was greater than the immediately adjacent left wheel path. In addition, for this site the mean delta was marginally greater for conventional porous asphalt compared to the epoxy-modified equivalent.

The presence of porosity in the asphalt layer is known to be a significant contributor to low-noise performance. No significant relationships were identified between the overall L_{CPX} and void fraction. A notable pattern was observed in the minimum L_{CPX} values, with a local minimum in the void fraction between 12.5 and 17.5%. It is recommended to explore this observed pattern further in a multivariate analysis.

Linear models were used to explore the relationships between each one-third octave band and void fraction. Negative correlations were observed in the 1,250 to 5,000 Hz bands. Potential mechanisms include increasing air flow permeability and acoustic absorption with increasing void fraction.

6 Preliminary Discussion of Mechanisms

The influences of void fraction on tyre/road noise generation and attenuation mechanisms are discussed in this section, albeit with a speculative tone due to the absence of supporting data.

The void fraction of a surface influences several of the dominant noise generation and attenuation mechanisms, specifically (1) air flow dispersion through the asphalt layer, (2) acoustic absorption, and (3) texture-induced vibration of the tyre (Sandberg & Ejsmont, 2002).

Air flow permeability is expected to be positively correlated with void fraction. Noise from turbulent air flow from "air pumping" is dominant in frequencies above approximately 1,000 Hz (Winroth et al., 2017). Increasing air flow permeability is anticipated to result in an overall reduction in high-frequency noise due to less turbulent aero-acoustic noise from air displacement.

For a porous absorber, the void fraction is theoretically positively correlated with the width of the peaks (Berengier et al., 1990), which is expected to manifest in reductions in tyre/road noise in specific frequency bands. The peak absorption bands are a function of layer thickness and void shape. For example, a surface with a thickness of 50 mm, specific air flow resistance of 20,000 Rayls/cm, and shape factor of 2.5, has theoretical absorption peaks at 1,077 and 3,226 Hz.

Texture, specifically the metric of MPD, is expected to be positively correlated with void fraction. The voids that are directly adjacent to the top surface of the layer are included in the calculation of MPD as they influence the overall mean depth of a segment (see ISO 13473-1:2019 for details of the measurement and calculation of MPD). Texture of chipseal surfaces was demonstrated to excite vibrations in the tyre (Fong, 1998), it is assumed that this mechanism can be translated to porous asphaltic mix surfaces, however the specific influence of texture due to voids is unknown.

Observations from the univariate analyses in this report include:

- In the 7 mm NMAS mixes, there was an indication of a minimum overall L_{CPX} at an estimated sub-surface void fraction (i.e., excluding surface voids) of approximately 15%.
- Negative correlations between L_{CPX} in the 1,250 to 5,000 Hz bands and void fraction.
- Positive correlation between MPD and void fraction within the 7 and 10 mm NMAS groups.

The hypothesised influences of void fraction on the L_{CPX} spectrum are:

- Positive correlation between void fraction and L_{CPX} in low frequencies due to increased texture.
- Mixed effects in mid-frequencies due to competing influences of texture-induced increase and absorption-induced decrease.
- Negative correlation between void fraction and L_{CPX} in high frequencies due to increased air flow permeability and acoustic absorption.

The univariate analyses in this report only exhibited the negative correlations in the high frequency bands (1,250 to 5,000 Hz). It was not possible to discern from the available data whether the relationships are due to decreased aero-acoustic noise, increased acoustic absorption, or another factor.

In situ measurement of the acoustic absorption using the method prescribed in ISO 13472-1:2022 would provide more direct insights into its impact on tyre/road noise, bypassing the indirect estimation through void fraction. The influence of void fraction on acoustic absorption could then be explored.

It is recommended to devise a method of measuring air flow permeability and investigating its relationship with void fraction and subsequent impact on tyre/road noise.

Furthermore, exploring how different types of tires (e.g., slick, heavy vehicle, etc.) interact with surface characteristics and subsequently tyre/road noise would be beneficial to ensure the observed relationships are not only limited to the P1 tyre.

References

Bell, G. (2024). *Road Noise Research—Effects of porous asphalt thickness, ageing, and epoxy, and CPX speed and tyre hardness* (23-117-R01). Altissimo Consulting Limited.

Berengier, M., Hamet, J. F., & Bar, P. (1990). Acoustical Properties of Porous Asphalts: Theoretical and Environmental Aspects. *Transportation Research Record*, *1265*. https://trid.trb.org/view/348600

Fong, S. (1998). Tyre noise predictions from computed road surface texture induced contact pressure. *INTER-NOISE and NOISE-CON Congress and Conference Proceedings*, *1998*(5), 828–831.

Noise and vibration research | Waka Kotahi NZ Transport Agency. (n.d.). Retrieved January 25, 2024, from https://www.nzta.govt.nz/roads-and-rail/highways-information-portal/technical-disciplines/environment-and-sustainability-in-our-operations/environmental-technical-areas/noise-and-vibration/noise-and-vibration-research/#road-surface-noise-research

Sandberg, U., & Ejsmont, J. A. (2002). *Tyre/Road Noise Reference Book*. https://trid.trb.org/view/730140

Winroth, J., Kropp, W., Hoever, C., Beckenbauer, T., & Männel, M. (2017). Investigating generation mechanisms of tyre/road noise by speed exponent analysis. *Applied Acoustics*, *115*, 101–108. https://doi.org/10.1016/j.apacoust.2016.08.027

Appendix A – Additional Data

Table 9: Longitudinal sample spacing for measurements in the wheel path.

Project	Surface Type	Carriageway	Lane	Spacing	Samples
CNC	EPA7 (30 mm)	SB	L2	10	39
				20	24
	EPA7 (50 mm)	SB	L1	10	38
			L2	10	92
	PA7 (30 mm)	SB	L2	20	11
		NB	R2	10	23
				20	36
	PA7 HS (30 mm)	NB	R2	20	17
	PA7 LV (30 mm)	NB	R2	20	19
	SMA7 (30 mm)	SB	L2	20	6
S2G	EPA10 (30 mm)	NB	R2	1	21
				10	28
	EPA10 HV (30 mm)			10	30
	EPA14 (30 mm)			20	14
WBB	EPA7 (30 mm)	NB	R2	10	26
	EPA7 (40 mm)			10	26
	EPA7 (50 mm)			1	21
				10	18

Table 10: Sample counts, mean, and standard deviation of void fraction measurements by project, surface type, and position.

Project	Surface Type	Position	Samples	Mean	SD
CNC	EPA7 (30 mm)	Lane 2	63	19.0	1.5
		Shoulder	23	20.6	1.6
	EPA7 (50 mm)	Lane 1	38	14.9	1.1
		Lane 2	92	17.0	1.4
		Shoulder	3	19.0	0.8
	PA7 (30 mm)	Lane 2	70	19.4	1.6
		Shoulder	23	22.0	1.2
	PA7 HS (30 mm)	Lane 2	17	14.1	1.7
		Shoulder	2	16.9	0.2
	PA7 LV (30 mm)	Lane 2	19	10.5	2.8
		Shoulder	2	13.0	2.7
	SMA7 (30 mm)	Lane 2	6	10.6	1.7
S2G	EPA10 (30 mm)	Lane 2	49	12.1	1.3
		Shoulder	9	18.7	3.0
	EPA10 HV (30 mm)	Lane 2	30	16.3	1.8
		Shoulder	5	19.9	2.1
	EPA14 (30 mm)	Lane 2	14	13.6	2.3
		Shoulder	6	19.0	0.9
WBB	EPA7 (30 mm)	Lane 2	26	13.2	1.3
		Shoulder	4	16.3	1.4
	EPA7 (40 mm)	Lane 2	26	14.1	1.0
		Shoulder	6	16.3	0.8
	EPA7 (50 mm)	Lane 2	39	14.0	0.9
		Shoulder	4	14.6	0.8

Appendix B – Road IDs and Reference Stations

Table 11: Project, Road ID and Reference Station (RS) mapping.

Project	Road ID	Reference Station
WBB	1715	01S-0327-D
S2G	3664	01S-0333/01.40-D
CNC	3843	074-0000-I
	3844	074-0000-D

Appendix C – Lane Labelling

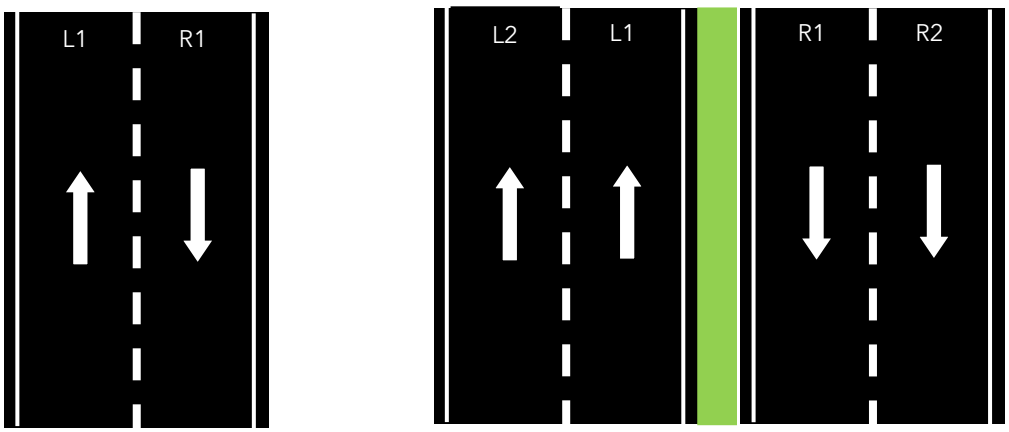

(a) Single carriageway (b) Dual carriageway

Figure 11. Lane labelling convention (assuming increasing direction toward the top of the page).